Experimental and Theoretical Investigations of Environmentally Sensitive Single-Molecule Fluorophores†

Katherine A. Willets,‡ Patrik R. Callis,§ and W. E. Moerner*,‡

Department of Chemistry, Stanford University, Stanford, California 94305, and Department of Chemistry and Biochemistry, Montana State University, Bozeman, Montana 59717

Received: January 21, 2004

The development of new fluorescent dyes for use in single-molecule imaging is an important challenge due to the numerous problems in biomolecular and materials science that can benefit from measurements at the level of individual molecules. A new class of fluorophores has been described recently that is not only well suited for single-molecule imaging but also shows strong sensitivity to the local environment. These molecules, known as the DCDHFs, contain an amine donor and a dicyanodihydrofuran acceptor linked by a conjugated unit (benzene, thiophene, styrene). The environmental sensitivity of these dyes can be characterized through bulk spectroscopic and fluorescence measurements as a function of solvent and solvent viscosity. Excited state lifetime data for single DCDHF molecules in polymers also demonstrate the value of the DCDHFs as probes of their local environment. To further understand the behavior, a series of electronic structure calculations have been completed, which yield insight into how certain twists within the DCDHF molecule may affect radiative and nonradiative processes. These insights will help direct synthetic modifications in the molecular structure to improve the environmental sensitivity and fluorescence quantum yield of these single-molecule probes.

1. Introduction

The development of new fluorescent dyes for use in single-molecule imaging is an important challenge due to the numerous problems in biomolecular and materials science that can benefit from insight at the level of individual molecules.[15,25,28,36] Fluorophores for single-molecule studies must have strong absorption, high fluorescence quantum yield, weak bottlenecks into triplet states, and high photostability.[24] While a number of fluorophores that meet these demands are available, the need for fluorophores with more specialized properties is growing. In particular, single-molecule fluorophores that can sense a variety of changes in their local environment would have widespread applications in both biological and polymer experiments.

Several classes of environmentally sensitive fluorophores are currently available, and these have been used primarily in bulk experiments. In the biological community, fluorophores are available for sensing pH, Ca^{2+} and other metallic ion concentrations, and membrane potentials.[13] Another class of fluorophores, the FLASH-type dyes, have a significant increase in fluorescence when they are bound to a particular peptide sequence with four cysteine residues versus the unbound state.[1] The fluorescence quantum yield of the naturally occurring fluorescent amino acid tryptophan is sensitive to its microenvironment within a protein and allows dynamics such as ligand/substrate binding and folding/unfolding processes to be studied.[5,31,32] The field continues to develop as several new fluorescent species with the ability to sense protein local environments have recently been reported.[6,30]

Single-molecule fluorophores report on the local environment by spectral shifts, changes in emission lifetime, degree of quenching, and orientational flexibility, to name a few possibilities. Changes in local pH affect the emission of the SNARF-1 dye,[3] and changes in local Ca^{2+} concentration can be sensed by Förster resonant energy transfer between a donor and an acceptor.[4] Another example is nile red, a laser dye with fluorescence properties that change upon introduction to different local environments.[7,29] Nile red has been used at the single-molecule limit to study molecular scale environments in polymer films[16] as well as to ascertain the effect of humidity on single-molecule dynamics.[17] The environmental sensitivity of crystal violet has also been exploited to study dynamics in thin polymer films.[39] As always, newer reporter dyes with single-molecule emission properties are needed, especially those with high photostability that are able to deliver more photons before photobleaching.

Understanding the origin of the environmental sensitivity of fluorescent dyes is a problem that has been addressed extensively in the literature. Studies on the mechanism behind the environmental sensitivity of nile red have focused primarily on the twisted intermolecular charge transfer (TICT) model, originally proposed by Grabowski to describe the dual fluorescence of dimethylaminobenzonitrile (DMABN).[11,12] In this model, molecules containing both an electron donor and acceptor are proposed to undergo an intramolecular charge transfer (ICT) followed by a rapid relaxation to a twisted state. In the case of DMABN, both the locally excited state and the TICT state are fluorescent allowing both states to be monitored in solvents of varying polarity and viscosity; however, in nile red, this does not appear to be the case. This has led to competing mechanisms to describe the environmental sensitivity of nile red, including contributions from hydrogen bonding.[7] Due to the wealth of

† Part of the special issue "Gerald Small Festschrift".
‡ Stanford University.
§ Montana State University.

10.1021/jp049684d CCC: $27.50
Published on Web 04/17/2004

potential changes in electronic structure that may lead to variable fluorescence properties, it is not always obvious what specific mechanism controls environmental sensitivity for a particular fluorophore system.

In this paper, we present experimental and theoretical studies on another class of environmentally sensitive single-molecule fluorophores, known as the DCDHFs. These molecules contain an amine donor and a dicyanodihydrofuran (DCDHF) acceptor linked by a conjugated unit (benzene, thiophene, alkene, styrene, etc.). We have recently reported this class of molecules as well suited for single-molecule imaging and have shown that the fluorescence quantum yield improves by a nearly an order of magnitude from toluene solution to a solid polymer host.[37] Here we explore the mechanism that leads to this environmental sensitivity, both through experimental and theoretical work. We first expand upon our measurements of the environmental sensitivity, demonstrating that the fluorescence properties vary in solvents of varying polarity and viscosity. This is followed by the results of a variety of electronic structure calculations. We then present a possible mechanism consistent with our results that may explain the environmental sensitivity. Our results yield insight into how certain twists within the DCDHF molecule may affect radiative and nonradiative processes. These insights will help direct synthetic modifications in the molecular structure to improve (or suppress) the environmental sensitivity and fluorescence quantum yield of these single-molecule probes, which then may be explored as reporters both in biological and materials science applications.

2. Materials and Methods

2.1. Experimental Methods. The DCDHF compounds were obtained from the laboratory of Professor Robert J. Twieg; the synthesis has been reported elsewhere.[14] Bulk absorption and emission spectra were measured using a Perkin-Elmer Lambda 19 UV−vis spectrometer and Fluoromax 2 fluorometer, respectively. For these measurements, a standard 1 cm path length quartz cuvette was mounted in the holder in the instrument. Solvents were of spectrophotometric grade from either J. T. Baker or Fisher Scientific. Fluorescence quantum yields were calculated using the previously reported value of DCDHF-6 in toluene[37] and corrected for differences in solvent refractive index.[19] Values for refractive indices, dielectric constants, and viscosities of the solvents were obtained from the CRC Handbook of Chemistry.[35] Fluorescence lifetime experiments were performed on a home-built confocal microscope based upon a commercial inverted microscope (Nikon TE300). Pumping radiation was provided by a frequency-doubled, mode-locked Ti-sapphire laser (Coherent Mira 900), wavelength tuned between 450 and 460 nm with a 75.7 MHz repetition rate and ~125 fs pulse. Emitted photons were discriminated from scattered pump photons with an 500LP long pass filter (Omega) and detected with a photon-counting avalanche photodiode (EG&G) equipped with a time-correlated single-photon counting (TCSPC) data analysis board (PicoQuant, TimeHarp 100 and TimeHarp 200). Full experimental details are described elsewhere.[38]

2.2. Theoretical Calculations. Calculations were performed using either the Gaussian 98 package (version A.7) or CAChe Worksystem Pro (version 6.01). For all quantum mechanical calculations, a 3-21g basis set was used. With the use of Gaussian 98, ground state geometries were optimized using the restricted Hartree−Fock (RHF) formalism, and dihedral angles defining various twists within the molecular structure were frozen using the popt keyword. Excited state energies and oscillator strengths were computed in G98 using two methods: first, Zerner's INDO/S (ZINDO/S) method[27,40] was applied to the optimized ground state structures; second, the CI-Singles (CIS) method[8,9] was used to determine the optimized geometry of the first excited state in addition to the excited state energies and oscillator strengths.

Additionally, semiempirical geometry optimizations and excited state energy calculations were performed using CAChe. Geometries were optimized with MOPAC using PM3 parameters and the heat of formation at the optimized geometry was recorded as a relative measure of ground state energy. ZINDO calculations were then done on these optimized geometries to obtain the excited state energies. CAChe uses a self-consistent reaction field solvent model to simulate the presence of solvent in its calculations by entering a dielectric constant, cavity radius, and refractive index (ZINDO only). For calculations in which the effect of solvent was included, the parameters associated with DMSO were used (see Table 1) and a cavity radius of 5 Å was chosen.

TABLE 1: Absorption and Emission Properties of DCDHF-6 in Various Solvents

solvent	Φ_F	λ_{abs}^{max} (nm)	λ_{em}^{max} (nm)	n[a]	ϵ_r[b]	Δf[c]	η[d] (cP)
			Aprotic				
acetonitrile	0.0030	495	531	1.3440	37.5	0.3055	0.345
acetone	0.0048	494	531	1.3570	20.7	0.2849	0.316
DMSO	0.011	504	543	1.4770	47.2	0.2640	2.24
THF	0.050	491	524	1.4040	7.52	0.2100	0.55
toluene	0.10	486	507	1.4940	2.379	0.0140	0.59
			Protic				
methanol	0.0051	496	531	1.3260	32.63	0.3095	0.597
ethanol	0.015	496	528	1.3590	24.3	0.2893	1.2
2-propanol	0.034	496	526	1.3776	18.3	0.2729	2.4
1-butanol	0.049	496	526	1.3993	17.1	0.2625	2.948
benzyl alcohol	0.072	505	537	1.5396	13.1	0.2061	5.8

[a] Refractive index. [b] Relative dielectric constant. [c] See text for definition. [d] Viscosity.

3. Results

3.1. Experimental Results. For the studies reported here, we have chosen DCDHF-6 as a representative member of the DCDHF class of molecules. The structure of DCDHF-6 is shown in Figure 1A. Single molecules of DCDHF-6 have been successfully imaged using an epi-illumination scheme described elsewhere.[24,38] Figure 1B shows an image of single DCDHF-6 molecules doped into a film of poly(methyl methacrylate) (PMMA) and excited at 488 nm. The integrated fluorescence intensity as a function of time for a single DCDHF-6 molecule is shown in Figure 1C, illustrating the high signal-to-background and stability of these molecules before the digital photobleaching characteristic of a single molecule. We are also able to measure the excited state lifetime of DCDHF-6 at the level of individual molecules. Parts D and E of Figure 1 show two sample TCSPC histograms for two different single molecules. The instrument response function (IRF, not shown) is deconvoluted from the data, and the data are fit to a single exponential using maximum likelihood estimation.[23] As these two fits show, the excited state lifetimes of the DCDHF-6 molecules vary depending on their local environment within the polymer film, demonstrating one type of sensitivity to local environment that we wish to address in this paper.

In order to explore the environmental sensitivity of the DCDHF molecules, bulk spectroscopic studies were performed on solutions of DCDHF-6 prepared in a variety of solvents,

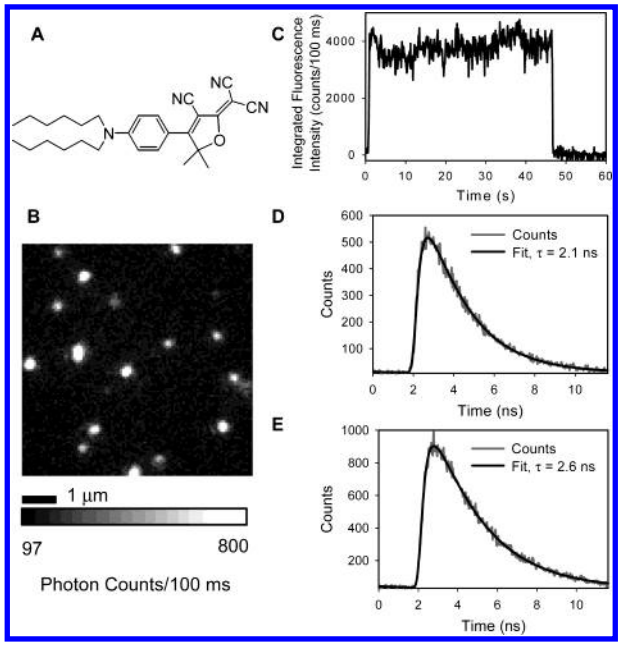

Figure 1. (A) Structure of DCDHF-6. (B) Single molecules of DCDHF-6 imaged in a PMMA film. The integrated fluorescence intensity of a single molecule as a function of time (C) and two examples of single-molecule TCSPC histograms (D) and (E) are shown for DCDHF-6 in PMMA. The lifetime data are fit to single exponentials using a maximum likelihood estimator and have decay times of 2.1 ns ($2I_r^* = 1.01$) and 2.6 ns ($2I_r^* = 1.09$), respectively.

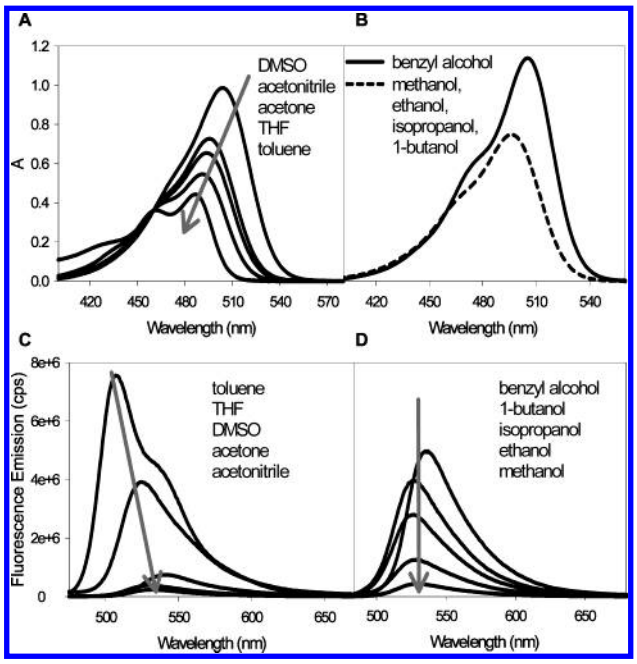

Figure 2. Absorption spectra of DCDHF-6 in a series of (A) aprotic and (B) protic solvents with constant absorption at $\lambda = 460$ nm. In part B, the absorption spectra of all alcohols except benzyl alcohol lie atop one another and are shown with a single dashed line. The emission spectra of DCDHF-6 are also shown in the same series of (C) aprotic and (D) protic solvents with $\lambda_{exc} = 460$ nm.

both protic and aprotic. The concentration of DCDHF-6 was adjusted so that all samples had the same optical density at 460 nm; this allows the overall (integrated) fluorescence intensity of the solutions to be compared directly when excited at this wavelength. Figure 2 shows the resulting absorption and emission spectra for DCDHF-6 in multiple solvents. This figure shows that the spectra become red shifted as the DCDHF-6 is introduced into more polar solvents. The overall fluorescence

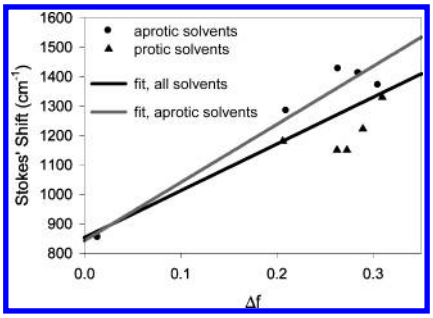

Figure 3. Lippert plot of (emission) Stokes' shift versus Δf for DCDHF-6 in all solvents in Table 1. The data are fit to a straight line for the case of all solvents (black line) and the aprotic solvents only (gray line). The slopes of the lines are 1588 cm^{-1} ($R^2 = 0.67$) and 1974 cm^{-1} ($R^2 = 0.95$), respectively.

intensity is also strongly affected by the identity of the solvent with toluene producing the strongest emission.

Table 1 summarizes the calculated fluorescence quantum yields and the wavelengths of maximum absorption and emission as well as several intrinsic solvent properties. Solvents are organized by their identity as either aprotic or protic and ordered by increasing DCDHF-6 fluorescence quantum yield within that grouping. The table reveals that the increase in fluorescence quantum yield is not universally linked to a similar trend in solvent refractive index, viscosity, or dielectric constant. The only parameter that does appear to correspond with the increasing quantum yields is Δf, defined as $(\epsilon - 1)/(2\epsilon + 1) - (n^2 - 1)/(2n^2 + 1)$.[19] As the fluorescence quantum yield increases within the solvent groupings, the value of Δf shows a corresponding decrease. However, hydrogen bonding also influences the value of the fluorescence quantum yield. Comparing two solvents with similar values of Δf but with different hydrogen-bonding ability—for example, the aprotic solvent DMSO and the protic solvent 1-butanol—reveals that the fluorescence quantum yield is higher in the solvent with the ability to hydrogen bond. Thus, Δf is not a sufficient parameter to describe the trends in the fluorescence quantum yield for all solvents.

In addition to changes in fluorescence quantum yield, the different solvents produce varying Stokes' shifts between the absorption and emission maxima for DCDHF-6. The Lippert equation uses a simple model of dipole−solvent interactions to relate the value of the Stokes' shift to the Δf of the solvent as follows:

$$\bar{\nu}_A - \bar{\nu}_F = \frac{2}{hc}\Delta f \frac{(\mu_E - \mu_G)^2}{a^3} + \text{constant} \qquad (1)$$

where $\bar{\nu}_A$ and $\bar{\nu}_F$ are the maximum absorption and emission energies in wavenumbers, μ_E and μ_G are the excited state and ground state dipole moments, respectively, and a is the Onsager cavity radius.[19] By fitting the experimental data to this equation and assuming a cavity radius of 5 Å, the excited state dipole moment of the DCDHF-6 can be determined. Figure 3 shows a Lippert plot for DCDHF-6 in all of the solvents listed in Table 1. A linear fit to the data for all solvents yields $|\mu_E - \mu_G| = 4.4$ D; using only the aprotic solvents in the fit increases this value to 5.0 D. The ground state dipole moment of this molecule is already significant, 11.4 D,[37] leading to values for the excited state dipole moment in the range of 15.8−16.4 D (since the hyperpolarizability β is positive, $\mu_E - \mu_G$ is positive). While these fits provide a framework for determining the excited state dipole moment, the data are quite scattered around the fits. This

suggests that the solvent-dependent behavior of DCDHF-6 cannot be simply modeled as dipole−solvent interactions.

Before moving to more complicated models to address the environmental sensitivity of the DCDHF molecules, we explored the possibility that multiple—and possibly nonfluorescent—species in solution could be contributing to the varying fluorescence quantum yield. To check for the presence of absorbing nonfluorescent species, the excitation spectra of DCDHF-6 were measured and compared to the absorption spectra of DCDHF-6 in different solvents. The two were found to overlap nicely, ruling out the possibility that nonfluorescent species were contributing to the absorption spectrum of the dye. The presence of dimers was checked separately by measuring solutions of DCDHF-6 in toluene at varying concentrations and then calculating the extinction coefficient at each concentration. The values of the extinction coefficients were the same regardless of the concentration of the original solution; thus dimer formation was ruled out as a possible contributing factor to the environmentally sensitive fluorescence. Lastly, the possibility of multiple fluorescent species was investigated for DCDHF-6. Fluorescence excitation spectra of DCDHF-6 in toluene were taken while monitoring emission wavelengths of 507 and 540 nm. The two spectra overlapped with one another as well as with the absorption spectrum for this system. This was repeated in DMSO, monitoring 540 and 560 nm, and identical results were found. As a final check, emission spectra with different excitation wavelengths were measured and again found to overlap. Thus, the possibility of multiple fluorescent species existing in solution was ruled out.

A key physical effect to consider is the influence that solvent viscosity has on the fluorescence of DCDHF-6. For these measurements, DCDHF-6 was added to glycerol/methanol solutions of varying concentrations. As the concentration of glycerol was increased, the absorption maximum shifted slightly from 496 nm at 0% glycerol to 505 nm at 83% glycerol (by volume). More striking, however, was the significant increase in DCDHF-6 fluorescence as the concentration of glycerol was increased. Figure 4A shows the emission curves for the DCDHF-6 fluorescence as the glycerol concentration is increased. From these data, the fluorescence quantum yield of the DCDHF-6 was calculated for each solution of increasing viscosity. Plotting the log of the fluorescence quantum yield against the log of the viscosity for both the glycerol/methanol solutions as well as the alcohols listed in Table 1 reveals a linear relationship between the two with a slope of 1.02 ($R^2 = 0.97$) as shown in Figure 4B. The relationship $\Phi_F \propto \eta^a$ has been explored extensively with the exponent a varying from 0 to 1.[2,10,20,22,33] Because $a = 1$ for our data, we can rule out several models such as the Förster−Hoffmann model for viscosity dependence which predicts a value of $a = {}^2/_3$.[10] Nevertheless, further work is needed to assign a specific mechanism for the relationship between the fluorescence quantum yield of the DCDHF molecules and the solvent viscosity. One additional observation is that this relationship between Φ_F and η only applies to the protic solvent data; in aprotic solvents, there is no clear correlation between the two.

While the mechanism governing the environmental sensitivity of the DCDHF molecules is not obvious from these experiments, the above results do demonstrate that the fluorescence quantum yield of DCDHF-6 is quite sensitive to its local environment, in particular to environmental rigidity. To demonstrate this, we exploited the well-known relationship between the fluorescence quantum yield and the excited state lifetime[19] and measured the excited state lifetime of DCDHF-6 in several different hosts.

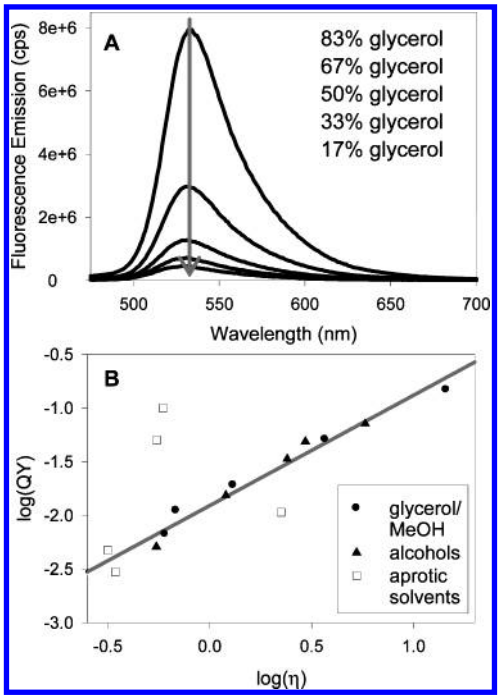

Figure 4. (A) Fluorescence emission of DCDHF-6 in solutions with increasing concentration of glycerol in methanol, $\lambda_{exc} = 460$ nm. (B) Log of fluorescence quantum yield as a function of the log of the viscosity (in cP). The data for the glycerol/methanol solutions (black circles) and the alcohols in Table 1 (black triangles) are fit to a line with a slope of 1.02 (gray line). The aprotic solvent data (open squares) are not included in this fit.

Figure 5A shows the ensemble excited state lifetime data for DCDHF-6 in toluene as well as in several different poly(alkyl methacrylate) polymers. The excited state lifetime in toluene is limited by the width of the instrument response function, measured to be 400 ps. However, the lifetimes of DCDHF-6 in the polymer films are much larger, in the nanosecond regime. The lifetime of the fluorophore increases as the glass transition temperature (T_g) of the host polymer increases, suggesting that this fluorophore is sensitive to inherent differences in the polymer environments. These results suggest these dyes may be useful as single-molecule probes of local environmental viscosity, rigidity, or free volume in polymer films.[21,41]

To explore this idea further, we measured the fluorescence lifetimes of 148 single molecules of DCDHF-6 in PMMA and 114 single molecules of DCDHF-6 in a (butyl methacrylate)/(isobutyl methacrylate) copolymer host. All molecules were checked for digital photobleaching to ensure that the collected emission was from a single molecule. Figure 5B shows a histogram of the lifetimes in each of these polymer hosts. Only molecules with more than 3000 counts were included in the histogram. On the basis of this minimum count number and the average excited state lifetime, as well as the number of channels used and the channel width of our detector, the statistically expected width of the histograms is ~100 ps.[23] Fitting the histograms to Gaussian distributions shows widths far greater than 100 ps for both polymers, which we attribute to microscopic heterogeneity of the polymer films. In PMMA, the mean of this fit was 2.5 ns with a fwhm of 0.70 ns; in the copolymer, the mean was 2.3 ns with a fwhm of 1.2 ns. The ensemble average value of the fluorescence lifetime is longer in PMMA than in the BM/*i*-BM copolymer, consistent with the bulk results above. In addition, the distribution of lifetimes is wider in the copolymer than in the PMMA host, suggesting a broader distribution of microscopic local environments in the

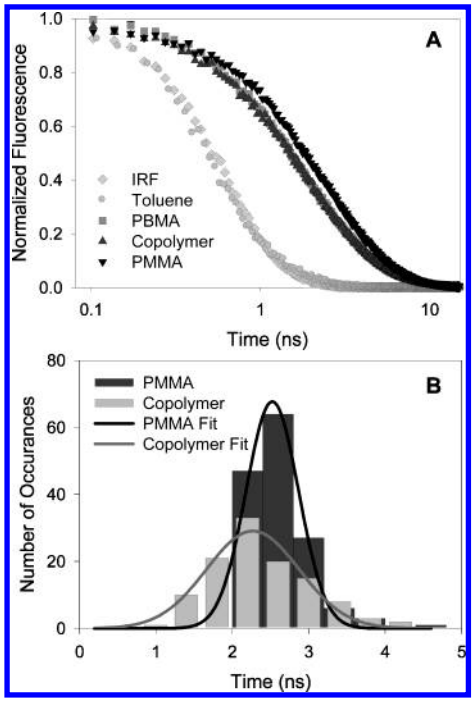

Figure 5. (A) Bulk lifetime data for DCDHF-6 in a series of solvent and polymer environments (log time axis). The polymer hosts are poly(*n*-butyl methacrylate), (PBMA, $T_g \sim 22$ °C); butyl methacrylate/isobutyl methacrylate copolymer (copolymer, $T_g \sim 35$ °C); and poly(methyl methacrylate), (PMMA, $T_g \sim 120$ °C). The shift toward longer lifetimes as the polymer host becomes more rigid demonstrates the sensitivity of this fluorophore to its environment. (B) Histogram of single-molecule fluorescence lifetimes of DCDHF-6 in the copolymer (light gray) and PMMA (dark gray). For both data sets, 400 ps bins are used. Data are fit to Gaussian distributions; fit parameters are given in the text.

copolymer. Because the fluorescence lifetime is sensitive to the identity of the polymer host, these dyes may prove useful for sensing dynamic changes in local environment, simply by monitoring changes in the excited state lifetime of an individual molecule as its host environment is perturbed.[38]

All of the experimental evidence presented above suggests a clear relationship between the local environment of the DCDHF-6 and its fluorescence properties. However, while some insight into the mechanism that drives this relationship is provided by these experiments, a more clear understanding of the specific structural changes in DCDHF-6 leading to nonradiative decay in certain environments would be useful. For this, we turn to theoretical studies of the DCDHF molecules.

3.2. Theoretical Results. Electronic structure calculations were performed in parallel with the experiments described above in an effort to explain the environmental sensitivity of the DCDHF molecules. For the calculations, DCDHF-1 was used as the model molecule instead of DCDHF-6; the two molecules are structurally identical except a simpler dimethylamine replaces the dihexylamine group. We chose to examine the effect of three specific twists on the energies of the ground and excited states of the molecule: (1) the amine−phenyl twist (α), (2) the phenyl−furan twist (ϕ), and (3) the dicyano−furan twist (δ). These three twists are defined by dihedral angles (α, ϕ, δ) respectively as shown in Figure 6A.

A gas-phase ground state geometry optimization (RHF/3-21g) on DCDHF-1 produces a structure with planar amine and dicyano groups with respect to the rings to which they are bonded, but with a $\phi \sim -40°$ twist between the phenyl and furan rings as shown in Figure 6A. This structure has a

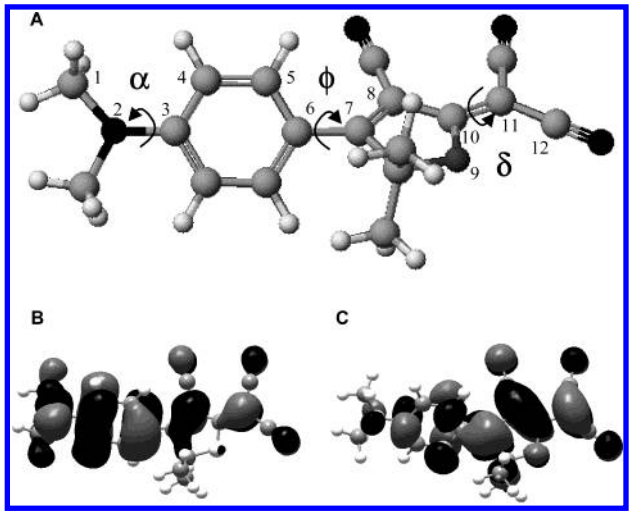

Figure 6. (A) Structure of DCDHF-1 with relevant dihedral angles for calculations shown. Twists around the amine−phenyl, phenyl−furan, and dicyano−furan bonds are denoted with angles α, ϕ, and δ respectively. The molecule is shown in the Γ_0 configuration where $\alpha = 1°$, $\phi = -39°$, and $\delta = 0°$. (B) HOMO and (C) LUMO of the DCDHF-1 molecule in the Γ_0 configuration calculated with RHF/3-21g.

calculated dipole moment of 15 D, which is slightly larger than the experimentally determined value of 11.4 D. We have chosen to refer to this lowest energy geometry as the Γ_0 structure for clarity in the following. All reported energies in this paper are referenced against the energy of Γ_0 (which is set to zero) unless otherwise indicated. The calculated HOMO and LUMO molecular orbitals for the Γ_0 structure are shown in parts B and C of Figure 6, respectively. While the electron density is localized more on the amine end of the molecule in the HOMO, it shifts to the dicyano end in the LUMO. Moreover, the bonding character changes for both the phenyl−furan and the dicyano−furan bonds between the HOMO and LUMO. Upon excitation, the phenyl−furan bond (bond 6−7 in Figure 6A) becomes more bonding, while the dicyano−furan bond (bond 10−11) becomes less bonding. On the other hand, the amine−phenyl bond (bond 2−3) does not appear to change dramatically in bonding character between the HOMO and LUMO.

To explore the roles of these three individual twists on the energy of the system, the dihedral angle defining a particular twist was frozen at a set value, and the ground state geometry was optimized while allowing all other parameters to vary freely. Table 2 summarizes the results from this series of calculations. There are several trends worth noticing in this table. First, as ϕ is varied, the energy of the molecule from its optimized ground state energy changes by less than 0.06 eV. This energy barrier is low enough that at room temperature the population of molecules existing in the fully twisted form ($\phi = -90°$) is about 10%; this suggests that the phenyl−furan bond can access all possible angles in the ground state at room temperature. This is not the case for changes in α and δ, where the accompanying changes in energy following the twists around the amine−phenyl or dicyano−furan bonds are large. Another important trend is that twisting around one particular bond often induces twisting around another bond. This is the case for both the amine−phenyl and dicyano−furan twists. Changes in both α and δ lead to subsequent changes in the value of ϕ. This result will have significance in later calculations.

With the use of these optimized geometries as the input structures, single-point S_1 energy calculations were performed with ZINDO to monitor how the excited state energies were

TABLE 2: Dihedral Angle Values and Ground State Energies of RHF/3-21g Optimized Gas-Phase DCDHF-1 at Certain Fixed Dihedral Angles

α	ϕ	δ	$E - E_{min}$ (eV)
		Fixed α	
1	*−39*	*0*	*0*[a]
15	−41	0	0.014
30	−43	0	0.065
45	−46	0	0.11
60	−51	0	0.14
75	−56	0	0.18
90	−61	0	0.21
105	−63	0	0.23
120	−63	0	0.23
		Fixed ϕ	
0	**0**	0	0.019
1	**−20**	0	0.0081
1	***−39***	*0*	*0*
1	**−70**	0	0.033
1	**−90**	0	0.052
		Fixed δ	
1	*−39*	***0***	*0*
1	−37	**15**	0.062
1	−35	**30**	0.24
1	−30	**45**	0.53
1	−23	**60**	0.90
1	−17	**75**	1.33
0	−10	**90**	1.76

[a] Values in italics correspond to the Γ_0 structure which has a minimum energy value of −978.0774 au. All energy values are referenced against this minimum energy.

affected by these different twists. After a vertical excitation induced from optical absorption, there are several mechanisms leading to nonradiative decay that could emerge from these results: (1) there could be two minima in S_1 leading to two possible excited state geometries, (2) the first and second excited states could cross leading again to different excited state structures, or (3) the ground and first excited state energies could cross allowing relaxation directly to the ground state by virtue of the large decrease in energy gap. Figure 7 shows the results from the ZINDO calculations as α, ϕ, and δ are varied, where the angles for Γ_0 are shown by the larger open squares. Considering the three mechanisms proposed above, there is no obvious crossing of states or multiple energetic minima that could lead to a nonfluorescent deactivation pathway. On the basis of these results, the (relaxed) excited state geometry is expected to have values of (α, ϕ, δ) = (0, 0, 0); that is, the structure of the DCDHF-1 is nearly planar in the first excited state. No other local minima appear to be present.

These results, however, are based on the optimized ground state structures calculated earlier. As mentioned previously, twists around certain bonds induce twists around other bonds in the optimized ground state geometries; thus, the possibility exists that for a given twist (i.e., fixed α or δ), the value of ϕ associated with the lowest energy conformation may be different for the ground and excited state structures. This suggests a need for excited state calculations where the geometry of the first excited state is optimized. Such calculations were completed using the CIS/3-21g formalism. With the use of the Γ_0 structure as the starting point, a CIS optimization to find the lowest energy first excited state geometry was performed. The resulting structure from this calculation is consistent with our expectations from the ZINDO calculations, that is, the molecule is nearly planar. When the energy of this first excited state relative to Γ_0 is calculated, the energy of the planar S_1 is 4.16 eV and the dipole moment is 19 D. We denote this particular structure $S_{1\phi}$ because it primarily involves a change in the angle ϕ (see Figure 8).

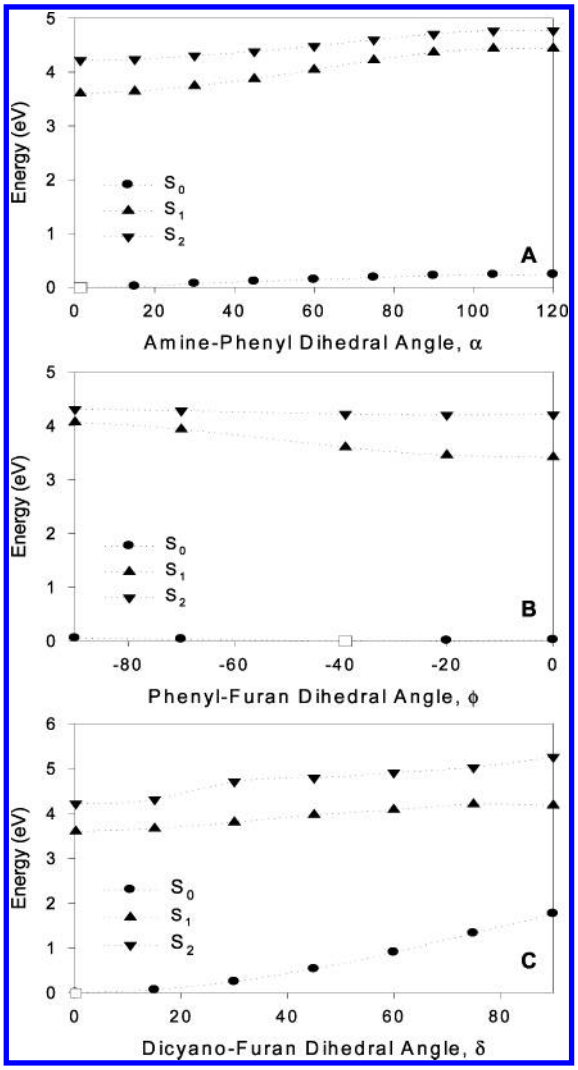

Figure 7. Ground and first and second excited state energies as a function of (A) amine−phenyl, (B) phenyl−furan, and (C) dicyano−furan dihedral angles. S_0 energies are calculated by RHF/3-21g using the popt keyword to fix the relevant dihedral angle. S_1 and S_2 energies are calculated with ZINDO on the ground state optimized structures. The open squares are the points corresponding to the Γ_0 structure. Lines are drawn to guide the eye.

The same CIS/3-21g calculation was repeated using the optimized ground state for the 90° dicyano−furan twist as the starting structure with an additional −20° twist of the phenyl−furan bond. The 90° dicyano−furan twist was chosen as the state of interest because the ZINDO calculations in Figure 7C show that the excited state energy for the case when δ = 90° is actually lower than that predicted for the δ = 75° twist, suggesting that a second excited state minimum may exist when the dicyano group is fully twisted. The results of this calculation reveal that a minimum does exist at this twisted geometry. The calculated energy of this additional first excited state relative to Γ_0 is 3.77 eV, and the calculated dipole moment is 10.6 D. This is actually lower in energy than the planar $S_{1\phi}$ first excited state found in the initial calculation. We denote this state $S_{1\delta}$ because it primarily involves a change in the value of the dicyano−furan twist angle (see Figure 8).

Performing similar calculations looking for additional excited state minima as a function of the amine−phenyl twist did not yield any additional first excited state structures of interest. The

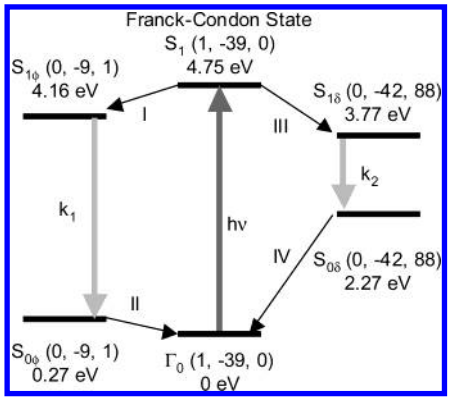

Figure 8. Proposed mechanism describing the various energy levels involved in the DCDHF-1 photophysics. Two first excited state energy minima exist for this molecule, one resulting from a twist in ϕ, the other from a twist in δ (denoted $S_{1\phi}$ and $S_{1\delta}$ respectively), allowing two different paths for deactivation.

ground state structure of the DCDHF-1 molecule with an amine−phenyl twist of 90° was used as a starting structure for this calculation, and the resulting first excited state geometry moved toward the planar geometry through subsequent iterations in the calculation. Thus, in the case of the DCDHF-1 molecule, no theoretical evidence has emerged from our calculations suggesting that a TICT state involving the amine group plays a role in its environmental sensitivity.

From these results, a mechanism can be proposed to describe the spectroscopic behavior of the DCDHF-1. Figure 8 shows a simplified picture of this mechanism. As the figure shows, the molecule can be excited from the Γ_0 state into a Franck−Condon state with a similar geometry to Γ_0. Given sufficient time, the molecule can relax into one of two excited state minima through either a change in ϕ or a change in δ. From either of these two excited states, the molecule can relax back down to the ground state, retaining its excited state geometry before relaxing back to Γ_0. Thus, there are two possible relaxation pathways from the Franck−Condon state. In the first, the phenyl and furan rings twist (path I) until reaching the $S_{1\phi}$ excited state geometry; from there, the molecule relaxes back to the ground state with rate constant k_1. This ground state geometry $S_{0\phi}$ has the same geometry as the $S_{1\phi}$ state, requiring another twist of the phenyl−furan bond to return to the Γ_0 structure (path II). The second relaxation pathway involves a twist of the dicyano group as the molecule moves from the Franck−Condon geometry to the $S_{1\delta}$ state (path III). From here, the molecule relaxes to the $S_{0\delta}$ ground state with rate k_2. Again, the geometry of $S_{0\delta}$ is the same as that of the $S_{1\delta}$ excited state, requiring a final twist of the dicyano group to return to the Γ_0 state (path IV). It is clear from the diagram that the energy difference between $S_{1\phi}$ and $S_{0\phi}$ is much larger than the gap between $S_{1\delta}$ and $S_{0\delta}$; we postulate that the latter transition is nonradiative based on our fluorescence data, which show only a single emission peak. If this transition were radiative, we would expect a second emission peak in the red region of the fluorescence spectrum. The presence of two excited state minima—one radiative and one nonradiative—is consistent with our environmentally sensitive fluorescence quantum yield. If the identity of the solvent favors the nonradiative $S_{1\delta}$ state, the fluorescence quantum yield of the molecule will be quite low; conversely, if the rotation of the dicyano group is slowed or prevented in a particular environment, the quantum yield will be much higher.

While the proposed mechanism in Figure 8 provides a simple picture to explain the behavior of DCDHF-1, it is by no means complete. Earlier calculations demonstrated that twists around the dicyano−furan and phenyl−furan bonds cannot be considered separately; thus we need to consider the full potential energy surface as a function of both dihedral angles simultaneously. For this, we chose to perform semiempirical geometry optimizations followed by ZINDO calculations on the resulting structures as they are far less computationally expensive. Before proceeding, a new lowest energy ground state (analogous to the Γ_0 state determined above) was calculated to use as a zero-energy point. Structures were then optimized using PM3 parameters for fixed values of ϕ and δ, and the ground and excited state energy surfaces were mapped out as a function of these angles. One caveat with the semiempirical optimizations is that there are notable structural changes from the HF/3-21g and CIS/3-21g optimized structures—namely, both the amine and dicyano groups (for $\delta > 0°$) become pyramidal rather than planar. In the case of the amine, this structural change is relatively unimportant, as our results have suggested that this group is not intimately involved with the fluorescence properties of the molecule. On the other hand, a change in the structure of the dicyano group could cause significant differences in our results. To compare this structural change to our earlier results, we examined CIS/3-21g optimized first excited states with different values of the dicyano twist—in the cases of intermediate δ, the dicyano group was pyramidal, but in the extreme cases of $\delta = 0°$ and 90°, the dicyano group was planar. Thus, for the PM3 geometry optimizations when $\delta = 90°$, an additional constraint was placed on the molecule, forcing the dicyano group to be planar in order to be consistent with the earlier CIS/3-21g results.

Figure 9B shows the S_0 potential energy surface as a function of ϕ and δ. This surface reinforces our earlier observation that in the ground state, ϕ is able to rotate while there is a significant barrier to rotation for δ. Figure 9A shows the S_1 potential surface as a function of ϕ and δ. Again, the surface is consistent with our earlier result that two excited state minima exist for DCDHF-1. However, these surfaces allow us to develop the mechanism suggested in Figure 8 more fully. The ground state surface indicates that the molecule can exist in a variety of ground state conformations; thus the Γ_0 ground state is really a distribution of states with varying values of ϕ. From this distribution of states, the molecule can be excited up to the S_1 potential surface, where it can access a variety of conformations as well. There appears to be no barrier from the distribution of Franck−Condon states accessible by vertical transitions to the $S_{1\phi}$ minimum energy state shown in Figure 8 as path I. On the other hand, path III in Figure 8 presents a more complicated picture as the molecule explores the potential surface from its Franck−Condon geometry toward the $S_{1\delta}$ state. As shown in Figure 9A, there is a ϕ-dependent activation barrier to the $S_{1\delta}$ state. At the thermodynamically favored value of $\phi = 0°$, this barrier is 0.33 eV. If this barrier is overcome and the dicyano group becomes fully twisted, there is a steep drop in the potential energy of the molecule, and it becomes trapped in the $S_{1\delta}$ conformation from which it can relax nonradiatively back to the ground state.

Because of the solvent sensitivity we have observed for the DCDHF molecules, we chose to perform the same set of calculations including simulated solvent. For this, parameters for DMSO were used because it is the solvent we have explored with the highest dielectric constant. The S_0 and S_1 potential surfaces as a function of ϕ and δ with solvent effects included are shown in parts B and A of Figure 10, respectively. The overall shape of S_0 is relatively unchanged from the gas-phase case in Figure 9B, and the trends noted above remain consistent. However, the shape of S_1 does change in the case where solvent

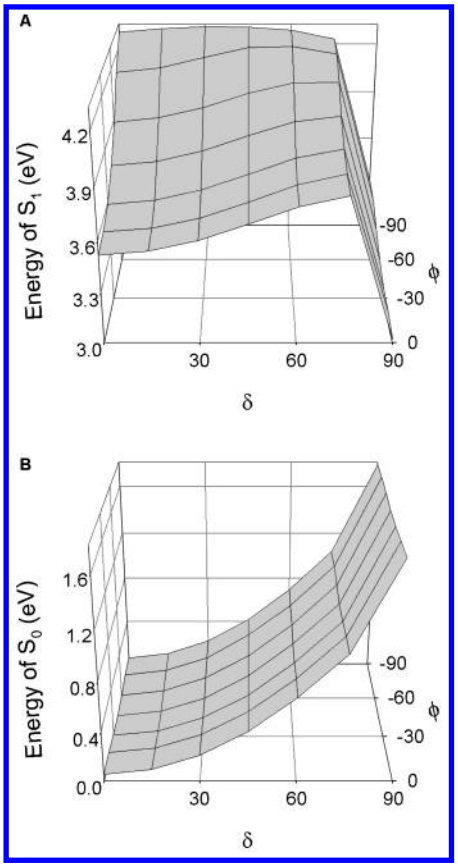

Figure 9. Potential energy surfaces of the first excited state (A) and ground state (B) of DCDHF-1 as a function of both the phenyl−furan and dicyano−furan dihedral angles. (B) was calculated using PM3 parameters and (A) from ZINDO on the PM3 optimized ground state structures. For the $\delta = 90°$ case, an additional constraint was placed on the molecule, forcing the dicyano group to be planar.

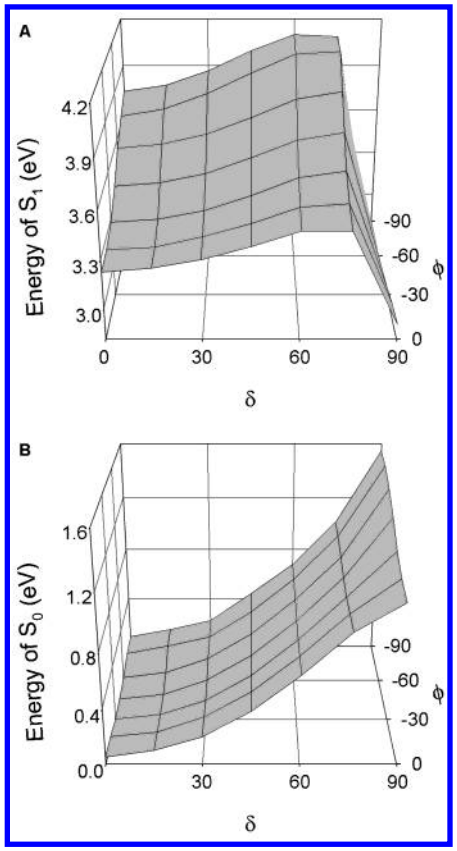

Figure 10. Potential energy surfaces of the first excited state (A) and ground state (B) of DCDHF-1 as a function of both the phenyl−furan and dicyano−furan dihedral angles with the effect of solvent included. (B) was calculated using PM3 parameters and (A) from ZINDO on the PM3 optimized ground state structures. For the $\delta = 90°$ case, an additional constraint was placed on the molecule, forcing the dicyano group to be planar.

is included. In the case when $\phi = 0°$, the barrier to rotation for the dicyano group is 0.25 eV in the simulated solvent rather than 0.33 eV in the gas phase. This reduction in the activation barrier to the $S_{1\delta}$ state suggests that the presence of the solvent increases the probability of the molecule entering the $S_{1\delta}$ state and relaxing nonradiatively. Therefore, while the overall mechanistic picture involving two excited state minima is preserved in this set of calculations, the barrier between the radiative and nonradiative excited states is reduced by the introduction of simulated solvent. As the activation barrier decreases, the $S_{1\delta}$ state becomes more accessible and the overall fluorescence quantum yield of the system will decrease.

4. Discussion

Combining the experimental and theoretical results reported in the previous section, we can now explore the mechanism proposed in Figure 8 in the context of our experimental data. The calculations have shown that two different twists in the DCDHF-1 molecule can lead to two different excited state minima: the twist around the phenyl−furan bond (ϕ) and the twist around the dicyano−furan bond (δ). From the Franck−Condon geometry, there is no barrier to the $S_{1\phi}$ state, and we have speculated that this leads to a straightforward radiative transition. However, the twist around the dicyano group follows a more complicated pathway to the nonradiative $S_{1\delta}$ state in which the value of ϕ plays a role in determining the barrier to rotation as described above. In the case when internal motion of the molecule is constrained (for example, in a rigid polymer film), the $S_{1\delta}$ state is not easily accessible, and we would expect the fluorescence quantum yield to be significantly higher than in solution. This is consistent with earlier results in which Φ_F of DCDHF-6 in PMMA was measured to be 0.92,[37] a significant improvement over the 0.10 value in toluene. When pushed toward a regime in which all internal motion is slowed (i.e., in more rigid solids and at very low temperatures), this value should approach unity.

Comparing our calculated dipole moments to those determined using the Lippert equation, we find that our calculated values are in good agreement with our experimental results. The fit to the Lippert equation shown in Figure 3 yields a value of $\mu_E - \mu_G = 4.4-5.0$ D. Our electronic structure calculations predict that the excited state dipole moment of the $S_{1\phi}$ state is 4 D higher than the dipole moment of the Γ_0 ground state. This is in sharp contrast to the $S_{1\delta}$ state where the dipole moment is actually 4.4 D *lower* than the Γ_0 ground state dipole moment (i.e., $\mu_E - \mu_G$ is negative). This further substantiates our claim that the $S_{1\phi}$ state is the path that leads to radiative decay due to the agreement between the experimentally determined and calculated values of $\mu_E - \mu_G$.

Returning to our experimental finding that $\Phi_F \propto \eta^a$ where $a = 1$, we can now consider different models that predict this particular relationship in the context of our proposed mechanism. In a simple hydrodynamic model such as the Debye−Stokes−Einstein equation, the rate of formation of a twisted state is inversely proportional to the solvent viscosity.[26,34] In the limit where the nonradiative rate is dominated by this rate of rotation (i.e., assuming that relaxation from the $S_{1\delta}$ state is instantaneous once formed) and where the nonradiative rate is much larger

than the radiative rate, this leads to the relationship between Φ_F and η that was determined experimentally. This is consistent with our proposed mechanism in which an intramolecular twist leads to a nonradiative transition although it neglects the thermodynamics of the situation.

It is worth noting additional models that predict $a = 1$ and consider the activation energy of the system. One such model is that of Kramers, which yields the desired result when evaluated at the Smoluchowski limit.[2,18] This, however, only applies in the high-barrier case, that is, when the barrier to rotation is significantly higher than *kT*. We have calculated this to be the case for the dicyano rotation when the phenyl−furan dihedral is small, that is, near zero. The model offered by Bagchi and co-workers predicts $a = 1$ in the case where a barrierless pinhole sink exists leading to radiationless decay.[2] This limit is only appropriate for the dicyano twist when ϕ is −90°, which is a low-probability geometry. Because these models predict rate constants, experiments in which the rates of radiative and nonradiative decay are measured would allow better fits to a particular model. Further, the calculations in which solvent was simulated suggest that a dielectric constant-dependent activation energy should also be included for a more complete treatment of the system.

Our results suggest that synthetic modifications of these molecules should target the furan end of the molecule rather than the amine if improvement of the fluorescence quantum yield is desired rather than environmental sensitivity. Although the twists around ϕ and δ are not independent of one another, our results do not suggest that simply constraining the phenyl−furan rotation will significantly improve the quantum yields. This is due to the fact that while the activation barrier is highest when the phenyl−furan rings are planar, the excited state with the 90° dicyano twist is still energetically favored. Thus, we believe that the more difficult task of preventing rotation around the dicyano group in the excited state is necessary for improving fluorescence quantum yields of the DCDHF molecules.

5. Conclusions

We have experimentally evaluated the environmental sensitivity of the DCDHF class of fluorophores across a range of protic and aprotic solvents and explored this sensitivity from a theoretical framework. The fluorescence quantum yield of the DCDHF follows a linear relationship with viscosity ($\Phi_F \propto \eta$) in protic solvents. Moreover, the excited state lifetime of single copies of DCDHF-6 is a sensitive parameter to probe the rigidity of a local polymer environment. Using electronic structure calculations, we have suggested that this environmental sensitivity is due to the presence of two excited state minima—one radiative and the other nonradiative. Depending on the host environment, the nonradiative state may be more or less favored, leading to respective decreases or increases in the fluorescence quantum yield. We believe that suppressing the internal rotational motion of the fluorophore through synthetic modification may lead to improved fluorescence quantum yields in solution. These results provide a foundation for interpretation of the behavior of these fluorophores in future single-molecule experiments in a variety of dynamic local environments.

Acknowledgment. The authors warmly thank Professor R. J. Twieg and Dr. M. He for providing the DCDHF derivatives and Dr. S. Hess for assisting with the lifetime measurements. This work has been supported in part by the National Science Foundation Grant No. DMR-0237247 (W.M.) and by Grant No. MCB-0133064 (P.C.).

References and Notes

(1) Adams, S. R.; Campbell, R. E.; Gross, L. A.; Martin, B. R.; Walkup, G. K.; Yao, Y.; Llopis, J.; Tsien, R. Y. *J. Am. Chem. Soc.* **2002**, *124*, 6063−6076.
(2) Bagchi, B.; Fleming, G. R.; Oxtoby, D. W. *J. Phys. Chem.* **1983**, *78*, 7375−7385.
(3) Brasselet, S.; Moerner, W. E. *Single Mol.* **2000**, *1*, 15−21.
(4) Brasselet, S.; Peterman, E. J. G.; Miyawaki, A.; Moerner, W. E. *J. Phys. Chem. B* **2000**, *104*, 3676−3682.
(5) Callis, P. R.; Liu, T. *J. Phys. Chem. A* **2004**, *108*, 4248−4259.
(6) Cohen, B. E.; McAnaney, T. B.; Park, E. S.; Jan, Y. N.; Boxer, S. G.; Jan, L. Y. *Science* **2002**, *2002*, 1700−1703.
(7) Cser, A.; Nagy, K.; Biczok, L. *Chem. Phys. Lett.* **2002**, *360*, 473−478.
(8) Foresman, J. B.; Frisch, Æ. *Exploring Chemistry with Electronic Structure Methods*, 2 ed.; Gaussian Inc.: Pittsburgh, PA, 1996.
(9) Foresman, J. B.; Head-Gordon, M.; Pople, J. A.; Frisch, M. J. *J. Phys. Chem.* **1992**, *96*, 135−149.
(10) Förster, T.; Hoffmann, G. *Z. Phys. Chem. NF* **1971**, *75*, 63−76.
(11) Ghoneim, N. *Spectrochim. Acta A* **2000**, *56*, 1003−1010.
(12) Grabowski, Z. R.; Rotkiewicz, K.; Rettig, W. *Chem. Rev.* **2003**, *103*, 3899−4031.
(13) Haugland, R. P. *Handbook of Fluorescent Probes and Research Products*, 9th ed.; Molecular Probes, Inc.: Eugene, OR, 2002.
(14) He, M.; Twieg, R.; Ostroverkhova, O.; Gubler, U.; Wright, D.; Moerner, W. E. *Proc. SPIE* **2002**, *4802*, 9−20.
(15) Higgins, D. A.; Hou, Y. Single Molecule Spectroscopy Used to Characterize Nanoscale Materials. In *Encyclopedia of Nanoscience and Nanotechnology*; James, A., Schwartz, C. C., Putyera, K., Eds.; Marcel Dekker: appearing 2003.
(16) Hou, Y.; Bardo, A. M.; Martinez, C.; Higgins, D. A. *J. Phys. Chem. B* **2000**, *104*, 212−219.
(17) Hou, Y.; Higgins, D. A. *J. Phys. Chem. B* **2002**, *106*, 10306−10315.
(18) Kramers, H. A. *Physica (The Hague)* **1940**, *7*, 284−304.
(19) Lakowicz, J. R. *Principles of Fluorescence Spectroscopy*; Kluwer Academic: New York, 1999.
(20) Law, K. Y. *Chem. Phys. Lett.* **1980**, *75*, 545−549.
(21) Loutfy, R. O. *Pure Appl. Chem.* **1986**, *58*, 1239−1248.
(22) Loutfy, R. O.; Arnold, B. A. *J. Phys. Chem.* **1982**, *86*, 4205−4211.
(23) Maus, M.; Cotlet, M.; Hofkens, J.; Gensch, T.; De Schryver, F. C.; Schaffer, J.; Seidel, C. A. M. *Anal. Chem.* **2001**, *73*, 2078−2086.
(24) Moerner, W. E.; Fromm, D. P. *Rev. Sci. Instrum.* **2003**, *74*, 3597−3619.
(25) Moerner, W. E.; Orrit, M. *Science* **1999**, *283*, 1670−1676.
(26) Rettig, W. *J. Phys. Chem.* **1982**, *86*, 1970−1976.
(27) Ridley, J.; Zerner, M. *Theor. Chim. Acta* **1973**, *32*, 111−134.
(28) *Single Molecule Spectroscopy: Nobel Conference Lectures*; Rigler, R., Orrit, M., Basche, T., Eds.; Springer Series in Chemical Physics; Springer-Verlag: Berlin, 2001; Vol. 67.
(29) Sackett, D. L.; Wolff, J. *Anal. Biochem.* **1987**, *167*, 228−234.
(30) Toutchkine, A.; Kraynov, V.; Hahn, K. *J. Am. Chem. Soc.* **2003**, *125*, 4132−4145.
(31) Vivian, J. T.; Callis, P. R. *Biophys. J.* **2001**, *80*, 2093-2109.
(32) Vivian, J. T.; Callis, P. R. *Chem. Phys. Lett.* **2003**, *369*, 409−414.
(33) Waldeck, D. H. Solute−Solvent Friction in Large-Amplitude Motions. In *Conformational Analysis of Molecules in Excited States*; Waluk, J., Ed.; Wiley-VCH: New York, 2000.
(34) Wandelt, B.; Turkewitsch, P.; Stranix, B. R.; Darling, G. D. *J. Chem. Soc., Faraday Trans.* **1995**, *91*, 4199−4205.
(35) *CRC Handbook of Chemistry and Physics*, 70 ed.; Weast, R. C., Ed.; CRC Press: Boca Raton, FL, 1989.
(36) Weiss, S. *Science* **1999**, *283*, 1676−1683.
(37) Willets, K. A.; Ostroverkhova, O.; He, M.; Twieg, R. J.; Moerner, W. E. *J. Am. Chem. Soc.* **2003**, *125*, 1174−1175.
(38) Willets, K. A.; Ostroverkhova, O.; Hess, S.; He, M.; Twieg, R. J.; Moerner, W. E. *Proc. SPIE* **2003**, *5222*, 150−157.
(39) Ye, J. J.; Ishikawa, M.; Yogi, O.; Okada, T.; Maruyama, Y. *Chem. Phys. Lett.* **1998**, *288*, 855−890.
(40) Zerner, M. Semiempirical Molecular Orbital Methods. In *Reviews in Computational Chemistry*; Lipkowitz, K. B., Boyd, D. B., Eds.; VCH: New York, 1991; Vol. 2, pp 313−366.
(41) Vallee, R. A. L.; Tomczak, N.; Kuipers, L.; Vansco, G. J.; van Hulst, N. F. *Phys. Rev. Lett.* **2003**, *91*, 038301.